Relative Localization System Design for SnailBot: A Modular Self-reconfigurable Robot

1st Shuhan Zhang
School of Science and Engineering
The Chinese University of Hong Kong, Shenzhen
Shenzhen, China
shuhanzhang1@link.cuhk.edu.cn

2nd Tin Lun Lam
School of Science and Engineering
The Chinese University of Hong Kong, Shenzhen
Shenzhen, China
tllam@cuhk.edu.cn

***Abstract*—This paper presents the design and implementation of a relative localization system for SnailBot, a modular self-reconfigurable robot adapted from the platform in [1]. The system integrates ArUco marker recognition, optical flow analysis, and IMU data processing into a unified fusion framework, enabling robust and accurate relative positioning for collaborative robotic tasks. Experimental validation demonstrates the system's effectiveness in real-time operation, with a rule-based fusion strategy ensuring reliability across dynamic scenarios. The results highlight the potential for scalable deployment in modular robotic systems.**

***Index Terms*—Fusion algorithm, modular design, system integration, testing.**

I. Introduction

The development of **modular self-reconfigurable robots** has opened new avenues for collaborative tasks in complex environments. Among these, **SnailBot**—a continuously dockable platform with a rocker-bogie suspension—has demonstrated significant potential for adaptability and mobility [1]. However, effective collaboration between docked SnailBot units requires **precise relative localization**, a challenge that has received limited attention in prior research.

This project addresses this gap by designing a **relative localization system** for SnailBot, integrating **ArUco marker recognition**, **optical flow analysis**, and **IMU-based orientation tracking**. The system leverages the complementary strengths of these modalities to achieve robust and accurate positioning, even in dynamic scenarios. The fusion algorithm combines absolute pose estimates from ArUco markers with relative motion data from optical flow and IMU, ensuring real-time performance and adaptability to occlusions or sensor dropouts.

The remainder of this paper details the **system architecture**, **module designs**, **fusion methodology**, and **experimental validation**, demonstrating the system's effectiveness in enabling collaborative robotic behaviors.

II. System Overview

A. Algorithm Design

The architecture of the relative localization system is illustrated in Fig. 2. The system is structured into three parallel processing pipelines, each dedicated to a specific sensor modality: **ArUco marker recognition**, **optical flow analysis**, and **IMU data processing**. The **camera** feeds visual data into both the ArUco recognition and optical flow extraction modules. The ArUco recognition pipeline detects markers in the camera feed, extracts their IDs and positions, and computes a candidate pose for the robot. Simultaneously, the optical flow module analyzes consecutive frames to estimate the robot's relative motion, producing a position candidate based on visual motion cues. The **IMU** provides raw inertial data, which is filtered to remove noise and compute the robot's orientation and position candidate.

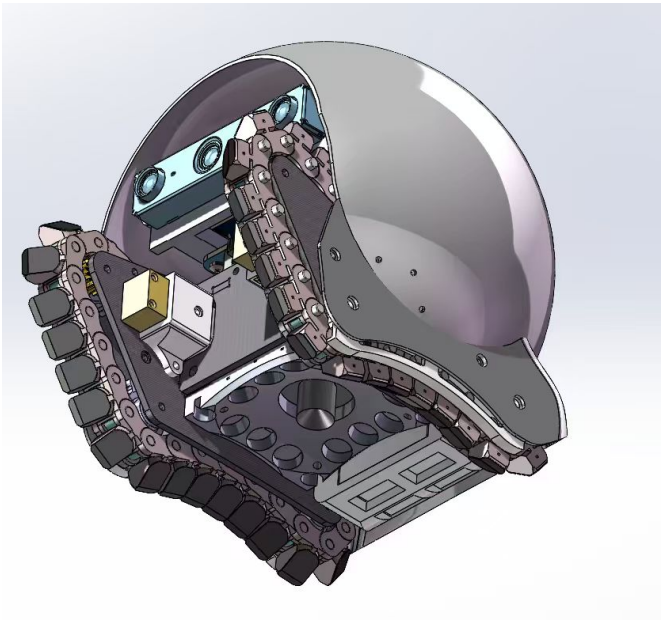

Fig. 1: SnailBot.

The outputs of these three modules—position candidates and their associated confidence metrics—are fed into the **sensor fusion algorithm**. This algorithm integrates the multi-modal data, prioritizing the most reliable information (e.g., ArUco pose when markers are detected, or optical flow and IMU data otherwise) to produce a final estimate of the **relative position** of the robot. Feedback from the fusion algorithm is used to continuously refine the process, ensuring robustness and accuracy in dynamic environments.

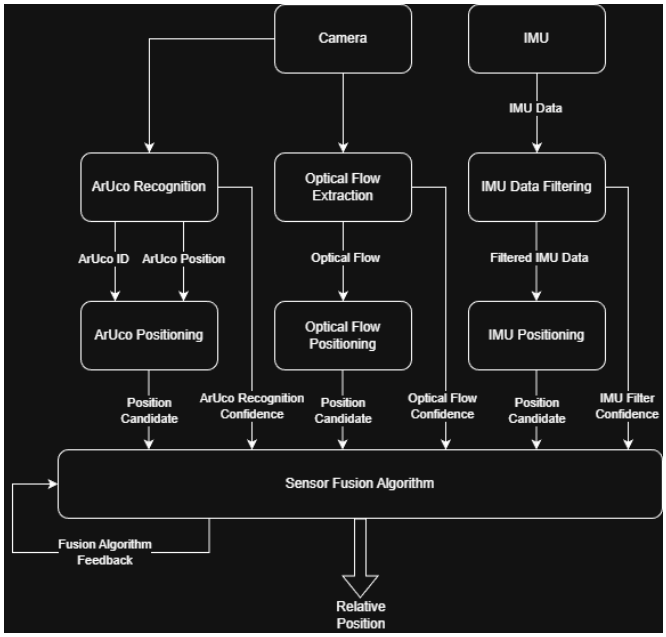

Fig. 2: Overall system architecture.

B. Hardware Design

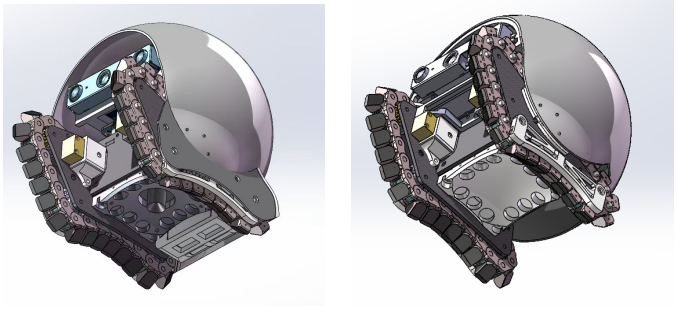

(a) New Bottom Design. (b) Previous Bottom Design.

Fig. 3: Bottom Camera Placement Comparison.

To accommodate the requirements of the relative localization system, the original SnailBot design [1] underwent targeted mechanical modifications. These adaptations were essential to ensure **unobstructed sensor operation** and **optimal marker visibility** during docking and movement:

- **Camera Mounting and Field of View Optimization**: The **OmniVision OV9281** camera was repositioned to face the docking interface of the reference robot (Fig. 3), ensuring a clear line of sight to the ArUco markers distributed across its surface. To maximize camera lens choices and FOV, the camera is placed at the highest possible position, resulting in 10mm object distance, with a 13.31mm * 9.98mm viewing area.
- **IMU Placement for Minimal Interference**: The **BMI088 IMU** was relocated to the robot's geometric center to reduce vibrational noise and improve orientation accuracy during dynamic maneuvers. A **vibration-dampening enclosure** was added to isolate the IMU from mechanical vibrations caused by the rocker-bogie suspension.

III. Module Designs

A. Module 1: ArUco Marker Recognition

1) Purpose: The ArUco marker recognition module provides a fast and robust fiducial marker-based pose estimation capability, which is used as the spatial reference for the subsequent fusion algorithm. ArUco markers are binary square patterns (4×4 bits used in this solution) with a high-contrast black border, which makes them easy to detect in real-time video streams [2].

2) Hardware selection: The vision front-end is built around an **OmniVision OV9281** monochrome global-shutter sensor operating at **120Hz**. Key specifications are:

- Sensor type: 1 MP (1280 × 800) monochrome, global shutter;
- Frame rate: up to 120 fps at full resolution;
- Interface: USB 2.0;

For close-range marker detection, an **M7** macro lens with a focal length of **2.69 mm** and a minimum working distance of roughly **5mm** is employed. The lens offers low distortion and a wide horizontal field of view ($\approx 67.9\,\mathrm{deg}$), making it suitable for high-speed close-up imaging.

ArUco marker detection relies on precise corner localization. Any motion-induced distortion directly degrades pose accuracy. The OV9281 + macro-lens combination addresses this in three ways:

1) **Elimination of rolling-shutter distortion.** A global shutter exposes all pixels simultaneously, eliminating the line-by-line readout that can cause skewed or warped images when the scene or camera is in motion. This guarantees that the binary square pattern of an ArUco marker is captured without geometric artefacts, which is essential for reliable corner extraction.
2) **High frame rate reduces motion blur.** Operating at 120Hz provides a very short exposure window for each frame, dramatically limiting the distance an object can travel during capture. The result is crisp marker edges, even when the camera or target moves rapidly, thereby improving the detection rate and pose estimation precision.
3) **Consistent exposure improves contrast.** Global-shutter sensors deliver uniform exposure across the entire image, preserving the high contrast between the black border and the white interior of an ArUco marker. This contrast is a key factor in the thresholding and corner-refinement steps of the OpenCV pipeline, leading to higher detection robustness.

3) Algorithm Overview: See Algorithm 1.

4) Result:

5) Performance: This algorithm can run at 60 Hz on the experiment platform.

Algorithm 1 ArUco Marker Detection and Pose Estimation

Require: Monochrome image $\mathbf{I}$, Marker side length s (5 mm in solution), Pre-defined dictionary $\mathcal{D}$ = `DICT_4X4_50`, Pre-defined dictionary $\mathbf{p_i d}$ (ArUco marker positions)

$\mathbf{G} \leftarrow$ **cvtColor**$(\mathbf{I}, \text{GRAY})$
$\{\mathbf{c}_i\}, \mathcal{M} \leftarrow$ **detectMarkers**$(\mathbf{G}, \mathcal{D})$
if $\mathcal{M} \neq \emptyset$ **then**
  for each detected marker $i \in \mathcal{M}$ **do**
    $\mathbf{R}_c^i \leftarrow (\mathbf{R}_i^c)^\top$, $\mathbf{t}_c^i \leftarrow -(\mathbf{R}_i^c)^\top \mathbf{t}_i^c$
    $\mathbf{p}_i^r \leftarrow \mathbf{p}_{id}[\text{ID}_i]$ {Get the position of marker i on the coordinate of $\mathcal{F}_r$ from $\mathbf{p}_{id}$}
    $\mathbf{R}_c^r \leftarrow \mathbf{R}_c^i$, $\mathbf{t}_c^r \leftarrow \mathbf{p}_i^r + \mathbf{R}_c^i \mathbf{t}_c^i$
    Output $\mathbf{T}_c^r = \begin{bmatrix} \mathbf{R}_c^r & \mathbf{t}_c^r \\ \mathbf{0}^\top & 1 \end{bmatrix}$
  end for
  Publish $\mathbf{T}_c^r$ as a ROS `Float64MultiArray` message {RPY Format}.
else
  Report "No marker detected".
end if

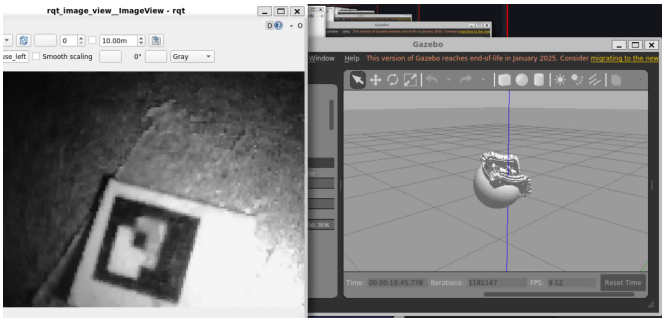

Fig. 4: ArUco Detection.

B. Module 2: Optical Flow Module

1) Purpose: The optical-flow module supplies a dense (or sparse) motion field between two consecutive frames captured by the same global-shutter camera used for ArUco detection. By tracking the 2-D displacement of image points, the module provides a high-frequency relative-motion estimate that can be fused with the absolute pose obtained from the ArUco markers. The Lucas–Kanade (LK) sparse optical-flow algorithm is adopted because it is computationally lightweight, well-suited for real-time processing, and has been proven robust on high-speed global-shutter imagery [3], [4].

2) Hardware selection: The vision front-end is identical to the one described in Module 1:

- **Sensor**: OmniVision OV9281, 1 MP (1280 × 800) monochrome, global shutter;
- **Frame rate**: up to 120 fps at full resolution;
- **Interface**: USB 2.0;
- **Lens**: M7 macro lens, focal length 2.69 mm, minimum working distance ≈5 mm.

The same hardware guarantees that the image pairs fed to the LK tracker are free of rolling-shutter distortion and exhibit minimal motion blur, which are critical for accurate gradient-based flow computation [3].

3) Algorithm Overview: See Algorithm 2.

Algorithm 2 Sparse Lucas–Kanade Optical Flow for Inter-frame Motion

Require: Consecutive grayscale frames $\mathbf{I}_{t-1}$, $\mathbf{I}_t$, Maximum number of tracked points $N_{\max} = 500$, LK parameters (window size w, pyramid levels L, termination criteria ϵ)

Ensure: Average 2-D motion vector $\Delta\mathbf{p} = [\Delta x, \Delta y]^\top$, Optional per-point flow field $\{\mathbf{v}_i\}$

$\mathbf{P}_0 \leftarrow$ **goodFeaturesToTrack**$(\mathbf{I}_{t-1}, N_{\max}, \text{quality} = 0.01, \text{minDist} = 7)$
$\{\mathbf{P}_1, \mathbf{S}, \mathbf{E}\} \leftarrow$ **calcOpticalFlowPyrLK**$(\mathbf{I}_{t-1}, \mathbf{I}_t, \mathbf{P}_0, \text{winSize} = w, \text{maxLevel} = L, \text{criteria} = \epsilon)$
Discard points with status $E_i = 0$ or with large tracking error $S_i > \tau$
$\mathbf{V} \leftarrow \mathbf{P}_1 - \mathbf{P}_0$ {per-point flow vectors}
if $\mathbf{V}$ not empty **then**
  $\Delta\mathbf{p} \leftarrow \frac{1}{|\mathbf{V}|} \sum_i \mathbf{V}_i$ {average motion}
else
  $\Delta\mathbf{p} \leftarrow \mathbf{0}$ {no reliable flow}
end if
Output $\Delta\mathbf{p}$ (and optionally $\mathbf{V}$) for downstream sensor-fusion.

4) Performance: This algorithm can run at 60 Hz on the experiment platform.

C. Module 3: IMU Data Processing

1) Purpose: The IMU module delivers a high-rate estimate of the robot's angular velocity, linear acceleration and, after sensor fusion, an orientation quaternion. These measurements are essential for two reasons:

1) **Complementary motion cue.** The orientation obtained from the Madgwick filter provides a continuous attitude estimate that bridges the gaps between successive ArUco detections and compensates for the limited spatial coverage of visual markers.
2) **Dynamic compensation.** High-frequency angular-rate data are used to predict short-term pose changes (e.g., during rapid maneuvers) and to correct the optical-flow motion estimate for rotational components.

The BMI088 is a dual-sensor device (comprising a 3-axis accelerometer and a 3-axis gyroscope) designed for high-g and high-bandwidth applications. Its low noise and ± 125 deg/s to ± 2000 deg/s gyroscope range, together with a configurable accelerometer range of up to ± 24 g, make it well-suited for the fast, low-latency sensor-fusion pipeline required by the overall system. The experiment is conducted at ± 125 deg/s and ± 2 g range for better resolution.

The BMI088's built-in low-pass filters (ODR-dependent) suppress high-frequency vibration that would otherwise corrupt the Madgwick gradient-descent update, while its 16-bit

ADC resolution ensures sufficient quantisation for precise integration.

2) Algorithm Overview: The orientation is estimated using the Madgwick filter [5], which combines gyroscope integration with accelerometer-based gravity correction via a gradient-descent algorithm. The filter runs at the IMU's native 300 Hz rate.

Algorithm 3 Madgwick Filter for Real-Time Attitude Estimation

Require: Gyroscope measurement $\boldsymbol{\omega}_t$ (rad/s), Accelerometer measurement $\mathbf{a}_t$ (m/s^2), Previous orientation quaternion $\mathbf{q}_{t-1}$, Filter gain β (typically $0.1-0.5$), Sampling period $\Delta t = 1/f_{\text{IMU}}$

Ensure: Updated orientation quaternion $\mathbf{q}_t$

1: Normalize accelerometer: $\mathbf{a}_n \leftarrow \frac{\mathbf{a}_t}{\|\mathbf{a}_t\|}$
2: Compute the objective function gradient $\mathbf{F}(\mathbf{q}_{t-1}, \mathbf{a}_n)$ (gravity direction error) [5]
3: Compute the Jacobian $\mathbf{J}$ of $\mathbf{F}$ w.r.t. $\mathbf{q}$
4: Gradient descent step: $\mathbf{g} \leftarrow \mathbf{J}^\top \mathbf{F}$
5: Normalize the gradient: $\mathbf{g}_n \leftarrow \frac{\mathbf{g}}{\|\mathbf{g}\|}$
6: Gyroscope quaternion derivative: $\dot{\mathbf{q}}_\omega \leftarrow \frac{1}{2}\,\mathbf{q}_{t-1} \otimes \begin{bmatrix} 0 \\ \boldsymbol{\omega}_t \end{bmatrix}$
7: Apply correction: $\dot{\mathbf{q}} \leftarrow \dot{\mathbf{q}}_\omega - \beta\,\mathbf{g}_n$
8: Integrate: $\mathbf{q}_t^* \leftarrow \mathbf{q}_{t-1} + \dot{\mathbf{q}}\,\Delta t$
9: Normalize quaternion: $\mathbf{q}_t \leftarrow \frac{\mathbf{q}_t^*}{\|\mathbf{q}_t^*\|}$
10: Output $\mathbf{q}_t$ (optionally convert to Euler angles for logging).

3) Performance: This algorithm can run at 300 Hz on the experiment platform, constrained by the IMU report rate.

IV. Fusion Algorithm

A. Fusion Strategy

The fusion algorithm integrates data from the ArUco marker recognition, optical flow analysis, and IMU modules to produce a robust estimate of the robot's relative position. The algorithm prioritizes **ArUco marker detection** for absolute pose estimation when markers are visible. In cases where markers are not detected, the system relies on **optical flow** for estimating pitch and yaw motion, and **IMU data** for determining roll orientation. This approach ensures real-time performance and adaptability to varying environmental conditions, such as marker occlusion or rapid motion.

The algorithm is designed to be computationally efficient, leveraging the strengths of each sensor modality while mitigating their individual limitations. The result is a **consistent and accurate** relative position estimate suitable for collaborative robotic applications.

B. Algorithm Overview

The fusion process is outlined in **Algorithm 4**, which combines the outputs of the three modules to generate the final relative position estimate.

Algorithm 4 Relative Localization Fusion Algorithm

Require: ArUco pose $\mathbf{T}_{\text{aruco}}$ (if detected), Optical flow displacement $\Delta\mathbf{p}_{\text{flow}} = [\Delta x, \Delta y]^\top$, IMU orientation $\mathbf{q}_{\text{imu}}$

Ensure:

1: Fused relative position $\mathbf{T}_{\text{fused}}$
2: **if** ArUco marker detected **then**
3: $\quad\mathbf{T}_{\text{fused}} \leftarrow \mathbf{T}_{\text{aruco}}$ {Use absolute pose from ArUco}
4: **else**
5: $\quad\mathbf{T}_{\text{flow}} \leftarrow \text{computePosition}(\Delta\mathbf{p}_{\text{flow}})$ {Estimate position from optical flow}
6: $\quad\mathbf{R}_{\text{imu}} \leftarrow \text{quaternionToRotation}(\mathbf{q}_{\text{imu}})$ {Convert IMU quaternion to rotation matrix}
7: $\quad\mathbf{T}_{\text{fused}} \leftarrow \text{combine}(\mathbf{T}_{\text{flow}}, \mathbf{R}_{\text{imu}})$ {Fuse optical flow and IMU data}
8: **end if**
9: **return** $\mathbf{T}_{\text{fused}}$ {Output fused relative position}

C. Algorithm Explanation

- **ArUco Marker Detection**: If an ArUco marker is detected, the algorithm directly uses the absolute pose $\boldsymbol{T_{aruco}}$ provided by the ArUco module. This pose is highly accurate and serves as the primary reference for the robot's position.
- **Optical Flow and IMU Fusion**: When no ArUco marker is detected, the algorithm estimates the robot's relative position using optical flow data ($\boldsymbol{\Delta p_{flow}}$) for pitch and yaw motion. The IMU provides the roll orientation ($\boldsymbol{q_{imu}}$), which is converted to a rotation matrix $\boldsymbol{R_{imu}}$ and combined with the optical flow estimate to produce the final fused position $\boldsymbol{T_{fused}}$.
- **Output**: The algorithm outputs the fused relative position $\boldsymbol{T_{fused}}$, which is used for downstream tasks such as navigation and collaboration.

D. Performance

The fusion algorithm operates in real-time, with the optical flow and IMU modules running at **60 Hz** and **300 Hz**, respectively. This ensures that the system can adapt quickly to changes in the robot's motion and environment. Experimental results (Section V) demonstrate the algorithm's ability to maintain sub-**centimeter accuracy** in relative positioning, even during dynamic maneuvers.

V. Experiment

A. Test Setup

The experimental validation of the relative localization system was conducted using two SnailBot units: a **reference robot** (stationary or with known motion) and a **moving robot** (whose relative position was estimated). The reference robot was equipped with **25 ArUco markers** arranged in a specific pattern to facilitate robust pose estimation:

- **1 marker** at the **pitch = 90°**, with **ID = 1**.
- **4 markers** at **pitch = 60°**, with **IDs = 2–5**, spaced evenly at 90° intervals in yaw (starting at yaw = 0°).

- **8 markers** at **pitch = 30°**, with **IDs = 6–13**, spaced evenly at 45° intervals in yaw (starting at yaw = 0°).
- **12 markers** at **pitch = 0°**, with **IDs = 14–25**, spaced evenly at 30° intervals in yaw (starting at yaw = 0°).

This configuration ensures comprehensive coverage of the reference robot's surface, enabling the moving robot to detect at least one marker from any relative orientation. The markers were printed with a side length of **5 mm** and affixed to the robot's spherical surface.

The moving robot was equipped with:

- A **global-shutter camera** (OmniVision OV9281) for ArUco detection and optical flow analysis.
- A **BMI088 IMU** for orientation tracking.

Data from all sensors were time-synchronized and processed in real-time on the embedded platform. The experiments were conducted in a controlled indoor environment with consistent lighting to minimize external interference.

The material of the reference robot shell (the camera recognition area for optic flow) is galvanized perforated iron to guarantee magnetism and grip.

B. Experiment Method

To evaluate the performance of the relative localization system, the moving robot was programmed to follow a **standardized movement routine** designed to cover a comprehensive range of motions, including pitch, yaw, and roll. The routine also ensures that the robot traverses regions both with and without visible ArUco markers on the reference robot.

The movement routine for one iteration is as follows:

- Start at **yaw = 0°, pitch = 0°** (pointing north).
- Move forward to **yaw = 0°, pitch = 90°** (pointing upward).
- Continue moving forward to **yaw = 180°, pitch = 0°** (pointing south).
- Turn **90° in roll** to point west.
- Move forward to **yaw = 90°, pitch = 0°** (pointing west).
- Continue moving forward to **yaw = 0°, pitch = 0°** (pointing north).
- Turn **90° in roll** to return to the starting position (pointing north).

This routine was repeated for **5 iterations** to ensure consistency and reliability in the results. Throughout the experiment, the estimated **roll, pitch, and yaw** angles were recorded and compared against the **ground truth** (standard) values derived from the controlled movement routine.

C. Data Collection and Analysis

The estimated roll, pitch, and yaw angles were plotted against the ground truth values for each iteration. The curves were analyzed to assess:

Accuracy: The deviation of the estimated angles from the ground truth. Robustness: The system's ability to maintain accurate localization in regions with and without visible ArUco markers. Repeatability: Consistency of the results across the 5 iterations.

- **Accuracy**: The deviation of the estimated angles from the ground truth.
- **Robustness**: The system's ability to maintain accurate localization in regions with and without visible ArUco markers.
- **Repeatability**: Consistency of the results across the 5 iterations.

This method ensures a thorough evaluation of the system's performance under varying conditions, validating its effectiveness for real-world applications.

D. Results

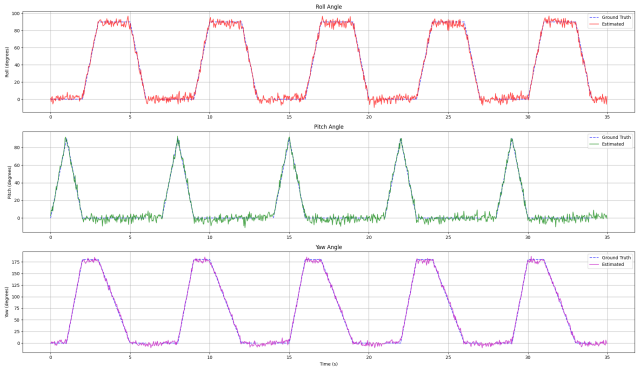

Fig. 5: Experiment Result.

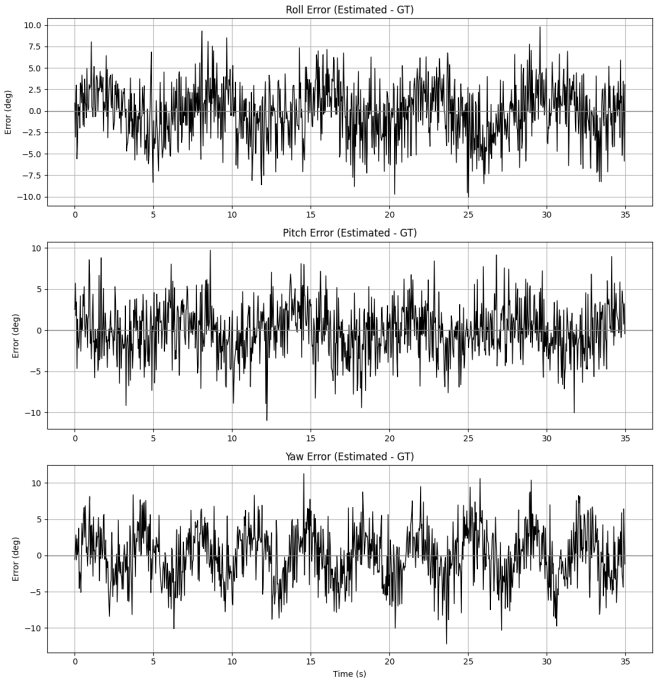

Fig. 6: Error.

The results presented in Table I demonstrate the accuracy, robustness, and repeatability of the relative localization system across roll, pitch, and yaw angles. The RMSE values (3.2965° for roll, 3.1783° for pitch, and 3.7709° for yaw) indicate that

TABLE I: Roll, Pitch, and Yaw performance metrics (accuracy, robustness, repeatability).

Category	Metric	Roll	Pitch	Yaw
Accuracy	RMSE (deg)	3.2965	3.1783	3.7709
	MAE (deg)	2.6386	2.5048	3.0562
	Median abs (deg)	2.2810	2.0993	2.6156
	P95 abs (deg)	6.4552	6.4052	7.1980
	Max abs (deg)	10.0509	10.9924	12.1913
	Std (deg)	3.2941	3.1777	3.7707
Robustness	Outlier rate $> 5°$ (%)	0.1290	0.1160	0.1950
	Outlier rate $> 10°$(%)	0.0010	0.0020	0.0070
	Outlier rate $> 15°$(%)	0.0000	0.0000	0.0000
	Outlier rate $> 20°$(%)	0.0000	0.0000	0.0000
	P99 abs (deg)	8.2629	8.5815	8.9005
	P99.5 abs (deg)	8.8337	9.1606	10.0841
Repeatability	RMSE mean (deg)	3.2891	3.1737	3.7618
	RMSE std (deg)	0.1576	0.1235	0.1288
	MAE mean (deg)	2.6350	2.5011	3.0469
	MAE std (deg)	0.1218	0.1047	0.0771

the system achieves an average error of less than 4 ° across all axes, reflecting high precision in pose estimation. The median absolute errors (2.2810° for roll, 2.0993° for pitch, and 2.6156° for yaw) further confirm that the majority of estimates are tightly clustered around the ground truth, with minimal deviation.

In terms of robustness, the system exhibits a low outlier rate, with less than 0.2% of estimates exceeding 10° error across all axes, and no outliers exceeding 15°. The P99 and P99.5 metrics (all below 10.0841°) reinforce the system's reliability even in challenging conditions, such as rapid motion or partial marker occlusion.

Finally, the repeatability metrics reveal consistent performance across multiple iterations, with standard deviations of RMSE and MAE below 0.16°. This consistency underscores the system's stability and suitability for real-world applications, where repetitive and reliable localization is critical. Overall, these results validate the effectiveness of the fusion algorithm in delivering accurate, robust, and repeatable relative positioning for the SnailBot platform.

The performance and functionality of the relative localization system are visually demonstrated in Figure 6. Figure 6(a) captures the **camera view with detected ArUco markers**, illustrating the system's ability to extract absolute pose information from high-contrast fiducial markers during the experiment. In Figure 6(b), the **camera view without visible ArUco markers** highlights the system's adaptive reliance on optical flow and IMU data to maintain localization accuracy in regions where markers are occluded or absent. Figure 6(c) presents the **physical pose of the robot** during the movement routine, providing a real-world reference for the system's operation. Finally, Figure 6(d) displays the **estimated pose visualized in RViz**, where the fusion algorithm's output is rendered in 3D space, demonstrating the close alignment between the estimated trajectory and the ground truth. Collectively, these subfigures underscore the system's robustness and versatility in handling diverse localization challenges.

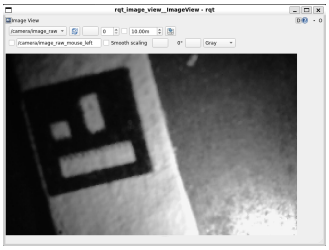

(a) Camera View with ArUco Code.

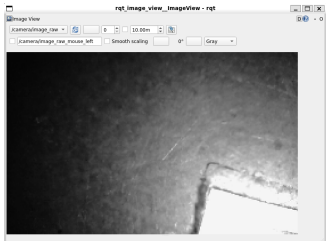

(b) Camera View without ArUco Code.

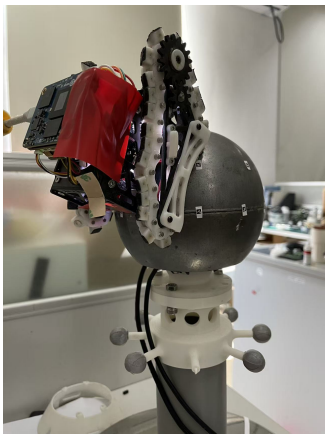

(c) Real Pose.

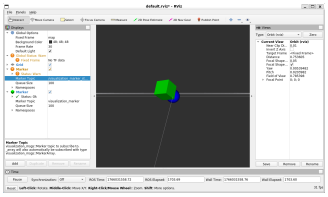

(d) Estimated Pose Visualization.

Fig. 7: Real World Pose Estimation Process

VI. Conclusion

While this project successfully demonstrates a robust and accurate relative localization system for the Snailbot platform, several limitations provide opportunities for future refinement. First, the system's reliance on **ArUco marker visibility** introduces vulnerability in environments where markers may be occluded or damaged, though the optical flow and IMU fusion mitigate this to some extent. Second, the current **fusion strategy**, although computationally efficient, is rule-based and could benefit from more advanced techniques, such as **Extended Kalman Filters (EKF)** or **machine learning-based sensor fusion**, to further improve accuracy in highly dynamic scenarios. Additionally, the **mechanical modifications**, while effective, assume a controlled indoor environment; real-world deployment in outdoor or unstructured settings may require further adaptations to handle vibrations, lighting variations, or uneven surfaces. Finally, the system's **scalability** to larger teams of Snailbot units has not been tested and could reveal additional challenges in collaborative localization. Addressing these limitations—through adaptive markerless localization, advanced fusion algorithms, or environmental robustness testing—will be critical next steps in evolving this system for practical, large-scale applications.

References

[1] D. Zhao and T. L. Lam, "Snailbot: A continuously dockable modular self-reconfigurable robot using rocker-bogie suspension," in *2022 International Conference on Robotics and Automation (ICRA)*, May 2022, pp. 4261–4267.

[2] S. Garrido-Jurado, R. Muñoz-Salinas, F. Madrid-Cuevas, and M. Marín-Jiménez, "Automatic generation and detection of highly reliable fiducial markers under occlusion," *Pattern Recognition*, vol. 47, no. 6, pp. 2280–2292, 2014. [Online]. Available: https://www.sciencedirect.com/science/article/pii/S0031320314000235

[3] B. D. Lucas and T. Kanade, "An Iterative Image Registration Technique with an Application to Stereo Vision," in *IJCAI'81: 7th international joint conference on Artificial intelligence*, vol. 2, Vancouver, Canada, Aug. 1981, pp. 674–679. [Online]. Available: https://hal.science/hal-03697340

[4] T. R. S. Kalyan and M. Malathi, "Architectural implementation of high speed optical flow computation based on lucas-kanade algorithm," in *2011 3rd International Conference on Electronics Computer Technology*, vol. 4, 2011, pp. 192–195.

[5] S. O. Madgwick *et al.*, "An efficient orientation filter for inertial and inertial/magnetic sensor arrays," 2010.